IMA Journal of Applied Mathematics (2013) **78**, 762–776
doi:10.1093/imamat/hxt021
Advance Access publication on May 14, 2013

A homotopy continuation approach for analysing finite-time singularities in thin liquid films

Dmitri Tseluiko*, Josh Baxter and Uwe Thiele
Department of Mathematical Sciences, Loughborough University, Leicestershire LE11 3TU, UK
*Corresponding author: d.tseluiko@lboro.ac.uk

[Received on 17 November 2012; revised on 7 April 2013; accepted on 8 April 2013]

We consider self-similar solutions related to rupture of thin liquid films on a solid substrate that evolve solely under the stabilizing influence of surface tension and the destabilizing influence of effective van der Waals interactions between the free surface of the film and the substrate. Such solutions have been previously analysed in the literature and various numerical approaches to obtain such solutions have been proposed. Such approaches are based either on shooting or finite-difference schemes and require well-chosen initial guesses for solutions. We propose an alternative numerical method, which is based on a homotopy approach and continuation techniques and allows one to reach self-similar solutions from analytically known small-amplitude steady solutions of the related thin-film equation. We argue that this method is more robust than previously proposed methods and does not require initial guesses to obtain solutions. Although the present study focuses on the particular case of self-similar solutions related to planar rupture that have square-root far-field behaviour, our approach can also be used to obtain planar solutions having a different far-field behaviour and radially symmetric self-similar solutions for the considered thin-film equation. We expect the approach to be also valid for other equations of similar type that show a subcritical primary bifurcation and finite-time singularities.

Keywords: thin films; self-similar solutions; homotopy approach.

1. Introduction

Thin liquid films play an essential role in a wide range of applications. They are important components in many technological processes, for example, in nanotechnology and chemical industries (see, e.g. Craster & Matar, 2009, and references therein), as well as in various biological settings, for example, in a human eye (where a liquid film protects the eye from dust and damaging particles as well as providing a lubricant for the eyelid to move across) (see, e.g. Sharma & Ruckenstein, 1985) and in the lining of the membrane of the lungs, which also contain thin liquid films (see, e.g. Grotberg & Jensen, 2004).

Thin films can show rich dynamics and a wide range of interesting phenomena, including regular and chaotic wave dynamics, fingering instabilities, rupture and dewetting (Oron *et al.*, 1997; Bonn *et al.*, 2009; Craster & Matar, 2009). In this paper, we focus on the rupture phenomenon, which is a finite-time singularity, i.e. the thickness of the liquid film tends locally to zero in finite time. It should be noted that rupture can occur not only in planar liquid films but also in other settings, for example, in liquid jets and threads (see, e.g. Papageorgiou, 1995; Eggers, 1997) and in free liquid sheets (see, e.g. Erneux & Davis, 1993; Ida & Miksis, 1996).

We analyse rupture of a thin film using a so-called thin-film equation. Such equations for films evolving on horizontal solid substrates are obtained under the approximation that the typical film thickness is much smaller than the lateral length scale over which variations in the film thickness occur, i.e. the equation results from a small gradient expansion. Such equations belong to the class of generalized

diffusion equations with the film thickness $h(x, y, t)$ being the diffusing field. They are of the form (Oron *et al.*, 1997; Thiele, 2010):

$$\frac{\partial h}{\partial t} = -\nabla \cdot \left[\frac{h^3}{3\mu} \nabla (\gamma \Delta h + \Pi(h)) \right], \tag{1.1}$$

where γ is the liquid–gas surface tension and μ is the dynamic viscosity of the liquid. The term $-\gamma \Delta h$ represents the Laplace pressure and the term $\Pi(h)$ stands for an additional pressure that may contain stabilizing and/or destabilizing influences resulting from hydrostatics, wettability, vertical temperature gradients, electric fields, etc. In the present study, we will solely consider the wettability effect, for which $\Pi(h)$ is the Derjaguin (or disjoining) pressure (Starov & Velarde, 2009) associated with attractive van der Waals forces between the molecules of the liquid and the substrate and modelled by $\Pi(h) = -\mathrm{d}g(h)/\mathrm{d}h$. Here, $g(h)$ is the local free energy per film area and is given by $g(h) = -A/(12\pi h^2)$, where A is the Hamaker constant associated with van der Waals forces (de Gennes, 1985; Israelachvili, 2011). Note that in this formulation, short-range repulsive forces are not taken into account and for $A > 0$ the disjoining pressure term is destabilizing and can lead to rupture in finite time. Here, we concentrate on the case of a 2D rupture that corresponds to a line rupture in the fully 3D situation.

The rupture phenomenon has been analysed in a number of previous studies. In particular, Zhang & Lister (1999) considered the same planar equation as in the present study and showed that the rupture occurs under the balance of destabilizing van der Waals forces and stabilizing surface tension forces. They derived equations for determining self-similar rupture solutions, $H(\eta)$, and showed that there exists a class of such solutions that satisfy the far-field behaviour $H \sim a\eta^{1/2}$. They also devised a numerical method based on shooting (with two shooting parameters) to obtain these self-similar solutions. It should be noted that this method requires good initial guesses for the shooting parameters to obtain the solutions. Zhang & Lister (1999) found a number of such self-similar solutions and suggested the existence of a countably infinite set of them characterized by a countable sequence $a = A_m$, $m = 1, 2, \ldots$, of proportionality factors in the far-field behaviour. Witelski & Bernoff (1999) proposed an alternative method based on a finite difference discretization and an under-relaxed Newton method. For convergence, such a method requires well-chosen initial guesses for the solutions. It should also be noted that Witelski & Bernoff (2000) found that the constants A_m satisfy the power-law scaling $A_m = O(m^{-k})$ as $m \to \infty$ with $k \approx 0.46$.

In this study, we propose an alternative method for computing self-similar rupture solutions. The method is based on homotopy continuation techniques (see, for example, Allgower & Georg, 1990). The advantage of this method is that it is a much more robust globally convergent method that does not require initial guesses to obtain the solutions. It utilizes the relation between the so-called critical nucleation solutions (that are unstable non-constant periodic solutions of the thin-film equation) and the self-similar rupture solutions. The relation of the critical nucleation solutions to rupture is that they serve as threshold solutions whose unstable manifolds (the instability of such solutions was rigorously shown by Laugesen & Pugh, 2000) in the direction of an increasing hole depth represent a time evolution towards rupture—perturbing a critical nucleation solution in this direction will lead to rupture while perturbing it in the opposite direction will lead to relaxation to a flat solution. In fact, it was rigorously shown by Laugesen & Pugh (2002) that critical nuclei are saddle points in the energy landscape (for an appropriate free energy functional). In the proposed method, we transform numerically by continuation the equation for obtaining critical nuclei with Neumann boundary conditions into the equation for computing self-similar rupture solutions with adequate boundary conditions, thereby transforming a critical nucleation solution into a self-similar rupture solution of a particular far-field behaviour. We additionally propose a strategy for obtaining a sequence of self-similar rupture solutions with the same type

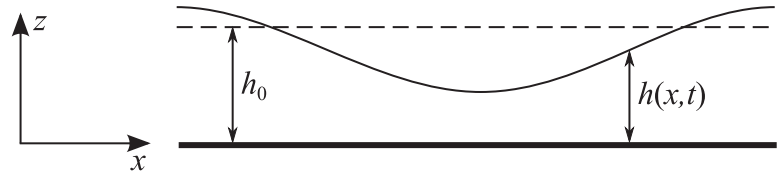

FIG. 1. Shown is a sketch of the considered thin liquid film on a smooth solid substrate.

of far-field behaviour in a single continuation run. In this way, we obtain a more complete sequence of such solutions when compared with previous studies. Our approach is limited by numerical noise resulting from rounding errors, which can be further suppressed and even more complete sequences of self-similar solutions can be found. Although we only apply our method to finding planar self-similar rupture solutions for a particular thin-film equation, it can be extended to analyse other types of finite-time singularity solutions in a wide variety of physical situations.

The paper is organized as follows. In Section 2, we discuss the model equation in detail. In Section 3, we analyse the linear stability of the film and discuss the subcritical branch of critical nucleation solutions bifurcating from the flat film. In Section 4, we discuss self-similar rupture of a liquid film and introduce an ordinary differential equation describing self-similar rupture solutions. In Section 5, we discuss a homotopy continuation method for obtaining self-similar rupture solutions and we present our results. Section 6 is devoted to conclusions.

2. Model equation

We consider a non-wetting liquid film on a horizontal smooth solid substrate; see Fig. 1. Wettability is modelled through a Derjaguin (or disjoining) pressure (de Gennes, 1985; Starov & Velarde, 2009) that only contains destabilizing van der Waals forces. Therefore, above a critical domain size the van der Waals forces overcome the stabilizing influence of surface tension, small disturbances to a uniform film thickness grow and subsequently result in film rupture. This situation exactly corresponds to the one studied by Williams & Davis (1982), Zhang & Lister (1999), Witelski & Bernoff (1999) and Witelski & Bernoff (2000).

We restrict our attention to the case of the rupture of a 2D film, corresponding to a line rupture in the fully 3D situation; see Witelski & Bernoff (2000). Then the free surface of the film is given by $z = h(x,t)$ in a suitably chosen Cartesian coordinate system (x,z) with the x-axis pointing along the substrate (Fig. 1). The dimensionless model equation we consider may be derived using a long-wave approximation (Oron *et al.*, 1997) based on the assumption that the wavelength of disturbances is much larger than the film thickness:

$$\partial_t h + \partial_x(h^3\partial_x[\partial_x^2 h + \Pi(h)]) = 0, \tag{2.1}$$

where $\partial_t = \partial/\partial t$ and $\partial_x = \partial/\partial x$. The term $-\partial_x^2 h$ represents the Laplace pressure and the term $\Pi(h) = -\mathrm{d}g(h)/\mathrm{d}h$ is the Derjaguin pressure resulting from van der Waals interaction between the molecules in the liquid film, the solid substrate and the ambient gas. Here, $g(h)$ is the local free energy per film area and is given by $g(h) = -1/(6h^2)$ (de Gennes, 1985; Israelachvili, 2011). The film thickness h has been non-dimensionalized using the undisturbed film thickness h_0, the coordinate x has been non-dimensionalized using $(2\pi\gamma/A)^{1/2}h_0^2$, where γ is the surface tension of the liquid, A is the Hamaker constant associated with van der Waals forces and t denotes time that has been non-dimensionalized

using $12\pi^2\mu\gamma h_0^5/A^2$, where μ is the dynamic viscosity of the liquid. Note that (2.1) can be written in the form

$$\partial_t h + \partial_x \left(h^3 \partial_x^3 h + \frac{1}{h} \partial_x h \right) = 0. \tag{2.2}$$

3. Steady-state solutions

First, let us analyse the linear stability of a flat film, $h \equiv 1$. We write $h(x,t) = 1 + \chi(x,t)$, where $|\chi| \ll 1$, and obtain the following linearized equation:

$$\partial_t \chi + \partial_x^4 \chi + \partial_x^2 \chi = 0. \tag{3.1}$$

Next, considering the ansatz $\chi \propto \mathrm{e}^{st+\mathrm{i}kx}$, we obtain the dispersion relation

$$s = k^2 - k^4. \tag{3.2}$$

We find that $s > 0$ if $|k| < 1$, i.e. the flat liquid film, $h \equiv 1$, is linearly unstable to disturbances with the wavenumber smaller than $k_c = 1$. If we consider (2.2) on a periodic domain of half-period L, then we find that the flat film solution $h \equiv 1$ is linearly stable for $L \leqslant L_c \equiv \pi/k_c = \pi$ and linearly unstable for $L > L_c$.

Next, we consider (2.2) on a periodic interval $[-L, L]$ and compute steady-state solutions $h = h_0(x)$, i.e. solutions satisfying

$$\left(h_0^3 h_0''' + \frac{h_0'}{h_0} \right)' = 0, \tag{3.3}$$

where primes denote differentiation with respect to x. Integrating this equation once, we find

$$h_0^3 h_0''' + \frac{h_0'}{h_0} = C_0, \tag{3.4}$$

where C_0 is a constant. Dividing by h_0^3, we obtain

$$\left(h_0'' - \frac{1}{3h_0^3} \right)' = \frac{C_0}{h_0^3}. \tag{3.5}$$

Integrating from $-L$ to L, we find for our periodic setting

$$0 = C_0 \int_{-L}^{L} \frac{1}{h_0^3} \, \mathrm{d}x. \tag{3.6}$$

Since h_0 is positive, $\int_{-L}^{L} (1/h_0^3) \, \mathrm{d}x > 0$. Therefore, $C_0 = 0$, i.e. h_0 satisfies the equation

$$\left(h_0'' - \frac{1}{3h_0^3} \right)' = 0. \tag{3.7}$$

Integrating once more, we find

$$h_0'' - \frac{1}{3h_0^3} = C_1, \tag{3.8}$$

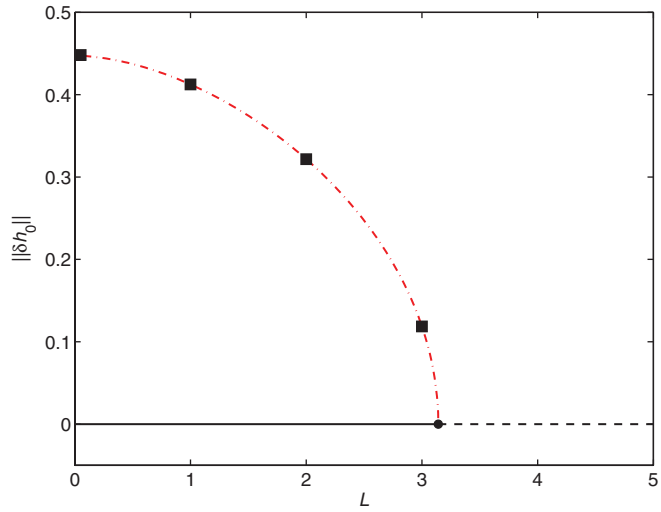

FIG. 2. Branches of steady-state solutions of (2.2). The solid, dashed and dot-dashed lines correspond to linearly stable constant solutions, linearly unstable constant solutions and linearly unstable non-constant solutions, respectively. The black squares correspond to $L = 3$, 2, 1 and 0.05 and indicate solutions whose profiles are shown in Fig. 3.

where C_1 is a constant, which (after one more integration) is found to be

$$C_1 = -\frac{1}{6L}\int_{-L}^{L}\frac{1}{h_0^3}\,\mathrm{d}x. \tag{3.9}$$

Solving (3.8) numerically, we obtain steady-state solutions, and it turns out that, for $L < L_c$, there exists a (subcritical) branch of unstable non-constant steady-state solutions, as can be seen in Fig. 2. It shows the dependence of the norm $\|\delta h_0\| = [(1/2L)\int_{-L}^{L}(h_0(x) - 1)^2\,\mathrm{d}x]^{1/2}$ on L. The dashed and solid horizontal lines correspond to linearly unstable and stable flat-film solutions, respectively, while the dot-dashed line corresponds to the unstable non-constant solutions. In fact, due to translational invariance of the equation and periodic boundary conditions, each point of the latter branch corresponds to an infinite number of steady-state solutions that are obtained from each other by translation in the x-direction. Therefore, the bifurcation at L_c is in fact a subcritical pitchfork of revolution. To eliminate this non-uniqueness, we can additionally require that $h_0(x)$ has a minimum at $x = 0$. Such non-constant solutions are shown in Fig. 3 for $L = 3$, 2, 1 and 0.05 by solid, dashed, dot-dashed and dotted lines, respectively. From the results proved by Laugesen & Pugh (2000), it follows that they are linearly unstable to perturbations of the same or a longer period. In fact, Laugesen & Pugh (2002) showed that these solutions are saddle points in the energy landscape with the free energy functional defined by

$$\mathcal{E}[h] = \int_{-L}^{L}\left(\frac{1}{2}(\partial_x h)^2 + g(h)\right)\mathrm{d}x, \tag{3.10}$$

where we remind that $g(h)$ is such that $\Pi(h) = -\mathrm{d}g(h)/\mathrm{d}h$. Here, the non-constant steady states have higher energy than the flat films (see Laugesen & Pugh, 2002), and are called critical nucleation solutions. Perturbing a non-constant steady state in one direction will lead to relaxation to a flat solution,

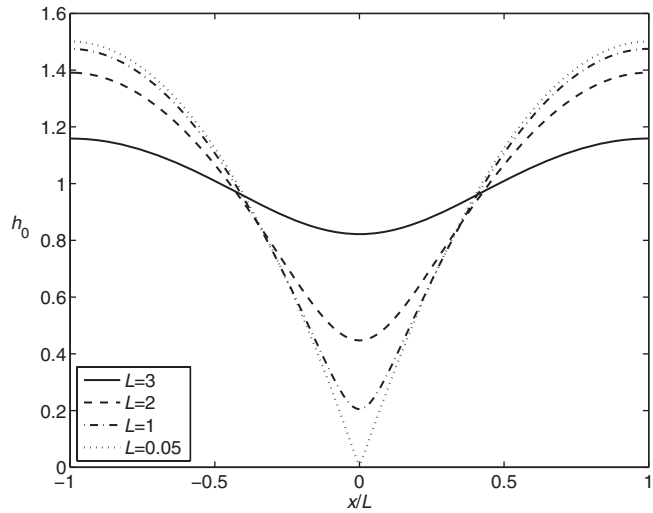

FIG. 3. Selected profiles of non-constant periodic steady-state solutions of (2.2) for $L = 3$, 2, 1 and 0.05 shown by solid, dashed, dot-dashed and dotted lines, respectively. The corresponding loci are indicated by black squares in Fig. 2.

while perturbing it in the opposite direction will lead to a rupture in finite time. We discuss a rupture of a liquid film in the next section.

4. Self-similar rupture

In time-dependent simulations (Williams & Davis, 1982; Zhang & Lister, 1999), it was shown that, for appropriate initial conditions, there is a finite-time singularity in the solution of (2.2) that corresponds to film rupture. In fact, the approach to singularity can be determined by self-similar solutions that are independent of initial and boundary conditions. Assuming that the liquid film ruptures at time $t = t_R$ at $x = 0$, it is found that the appropriate self-similar solution ansatz is

$$h(x,t) = (t_R - t)^{1/5} H(\eta), \quad \eta = \frac{x}{(t_R - t)^{2/5}}. \tag{4.1}$$

Substituting (4.1) into (2.2), Zhang & Lister (1999) obtained the ordinary differential equation

$$\frac{1}{5}(H - 2\eta H') = \left(\frac{H'}{H} + H^3 H'''\right)', \tag{4.2}$$

where primes denote differentiation with respect to η. The analysis of film rupture reduces to analysing solutions of this equation. Additionally, symmetry conditions are imposed at $\eta = 0$:

$$H'(0) = 0, \quad H'''(0) = 0. \tag{4.3}$$

One also needs to determine the far-field behaviour at $\eta \to \infty$. Close to rupture, the changes in the minimal film height (at $x = \eta = 0$) occur much more rapidly than the changes in the film height away

from the rupture point. This implies that, as $t \to t_R^-$, the quasi-steady assumption

$$\frac{\partial h}{\partial t} \sim 0 \tag{4.4}$$

should hold at fixed x away from the rupture point (Zhang & Lister, 1999). Applying re-scaling (4.1), this corresponds to $\frac{1}{5}(H - 2\eta H') \backsim 0$ as $\eta \to \infty$, which implies

$$H(\eta) \backsim a\eta^{1/2} \quad \text{as } \eta \to \infty, \tag{4.5}$$

where a is a constant to be found.

Let H be a solution satisfying conditions (4.3) at $\eta = 0$ and the far-field condition (4.5) for some constant a. The linear stability analysis of such a solution shows that there are two growing modes as $\eta \to \infty$. In our numerical computations on finite but large domains, $\eta \in [0, L]$, the fact that there are two growing modes leads to the need of two boundary conditions at $\eta = L$ to eliminate these growing modes. As in Zhang & Lister (1999), we use the conditions

$$H - 2LH' = 0, \quad H + 4L^2 H'' = 0, \tag{4.6}$$

that are both consistent with condition (4.5). Note, however, that other choices are possible.

5. Determining self-similar rupture solutions

To compute self-similar rupture solutions satisfying conditions (4.3) and (4.5), Zhang & Lister (1999) proposed a numerical shooting scheme based on a fourth-order Runge–Kutta method with two shooting parameters, $H(0)$ and $H''(0)$. Initial guesses for $H(0)$ and $H''(0)$ were chosen to start the shooting and the parameters were adjusted to satisfy conditions (4.6). A search for such solutions lead to isolated points in the $(H(0), H''(0))$-plane and it was suggested that there is an infinite countable set of such self-similar solutions, which have $a = A_m$, $m = 1, 2, \ldots$, in (4.5). Witelski & Bernoff (1999) proposed an alternative method based on a finite difference scheme on a finite but large domain and solved via an under-relaxed Newton method. It should be noted that for convergence such methods need well-chosen initial guesses for solutions. Moreover, Witelski & Bernoff (2000) found that the A_m's satisfy the power-law scaling $A_m = O(m^{-k})$ as $m \to \infty$ with $k \approx 0.46$.

Here, we propose a much more robust globally convergent method for computing such solutions. The method is based on homotopy continuation techniques and does not require initial guesses to obtain solutions. We employ the continuation and bifurcation toolbox AUTO-07P (Doedel *et al.*, 1991; Doedel & Oldeman, 2009). The first step is to utilize the relation of the critical nucleation solutions discussed in Section 3 to self-similar rupture solutions. Both are related to rupture: the former are threshold solutions whose unstable manifolds represent (in the direction of increasing hole depth) a time evolution towards rupture. In particular, at small L the solutions are already close to rupture (see Fig. 3). Based on this observation, roughly speaking, we use a homotopy approach that transforms (3.3) for determining nucleation solutions with 'incomplete' Neumann boundary conditions (see below) into (4.2) for self-similar solutions with conditions (4.3) and (4.6). Thereby, we transform a nucleation solution into a self-similar solution. To formulate this more precisely, we introduce the family of ordinary differential equations that depends on parameter A:

$$f'''' = \frac{A}{5}\left(\frac{1}{f^2} - \frac{2\xi f'}{f^3}\right) - \frac{f''}{f^4} + \frac{(f')^2}{f^5} - \frac{3f'f'''}{f}. \tag{5.1}$$

Here, f is a function of ξ and primes denote differentiation with respect to ξ. For $A=0$, we obtain (3.3) with x and h_0 being identified with ξ and f, respectively. In contrast, for $A=1$, we obtain (4.2) with η and H being identified with ξ and f, respectively. We consider (5.1) on an interval $\xi \in [0, L]$, and introduce the boundary conditions

$$f'(0) = 0, \tag{5.2}$$

$$f'''(0) = B, \tag{5.3}$$

$$C f(L) - L f'(L) = 0, \tag{5.4}$$

$$C(C-1) f(L) - L^2 f''(L) = D, \tag{5.5}$$

with three more parameters, B, C and D whose usefulness will become clear later. The integral condition

$$\frac{1}{L}\int_0^L f \, \mathrm{d}\xi = 1 \tag{5.6}$$

fixes the mean film thickness.

On the one hand, (5.1) with $A=0$ along with boundary conditions (5.2–5.4) where $B=C=0$ and integral condition (5.6) constitutes a well-posed boundary-value problem for finding the critical nucleation solutions discussed in Section 3. On the other hand, (5.1) with $A=1$ along with boundary conditions (5.2–5.5) where $B=0$, $C=\frac{1}{2}$ and $D=0$ constitutes a boundary-value problem for determining the self-similar rupture solutions discussed in Section 4.

To use the continuation toolbox AUTO-07P, we first write (5.1) as a system of first-order autonomous ordinary differential equations on the interval $[0, 1]$. Therefore, we introduce the variables $y_1 = f$, $y_2 = f'$, $y_3 = f''$, $y_4 = f'''$ and $y_5 = \xi$, and obtain from (5.1):

$$\dot{y}_1 = L y_2, \tag{5.7}$$

$$\dot{y}_2 = L y_3, \tag{5.8}$$

$$\dot{y}_3 = L y_4, \tag{5.9}$$

$$\dot{y}_4 = L\left[\frac{A}{5}\left(\frac{1}{y_1^2} - \frac{2y_5 y_2}{y_1^3}\right) - \frac{y_3}{y_1^4} + \frac{y_2^2}{y_1^5} - \frac{3y_2 y_4}{y_1}\right], \tag{5.10}$$

$$\dot{y}_5 = L, \tag{5.11}$$

where dots denote derivatives with respect to $\rho \equiv \xi/L$. The advantage of the used form is that the fields $y_i(\rho)$ correspond to the correctly scaled dependent and independent physical variables that all depend only on the internal variable $\rho \in [0, 1]$. The boundary conditions take the form

$$y_2(0) = 0, \tag{5.12}$$

$$y_4(0) = B, \tag{5.13}$$

$$C\, y_1(1) - L\, y_2(1) = 0, \tag{5.14}$$

$$C(C-1) y_1(1) - L^2 y_3(1) = D. \tag{5.15}$$

In addition, we need to impose the condition

$$y_5(0) = 0 \tag{5.16}$$

that 'pins' the physical independent variable. The integral condition takes the following form:

$$\int_0^1 y_1 \, \mathrm{d}\rho = 1. \tag{5.17}$$

As was mentioned above, this condition is used only for computation of critical nucleation solutions and is not needed for computation of solutions determining rupture discussed in Section 4.

Note that the dimension of the problem (5.7–5.11) is $N_{\mathrm{dim}} = 5$, the total number of boundary conditions is $N_{\mathrm{bc}} = 5$, the number of integral conditions is $N_{\mathrm{int}} = 1$ and parameters are $L, A, \ldots, D$. So, for each continuation run, $N_{\mathrm{bc}} + N_{\mathrm{int}} - N_{\mathrm{dim}} + 1 = 2$ parameters should be free (see Doedel & Oldeman, 2009) and the remaining parameters must be fixed.

Let us first consider computation of nucleation solutions using as the starting solution the small-amplitude sinusoidal profile, $y_1 = 1 - 0.001\cos(y_5)$, that represents an approximate analytical solution at $L = L_c = \pi$ (we fix $A = 0$, $B = 0$ and $C = 0$ during this continuation run). The fields y_2, y_3 and y_4 are chosen appropriately and $y_5 = L_c\rho = \pi\rho$. Then we decrease L and let D adapt. Note that the initial value of D is taken to be zero. This run reproduces results shown in Figs 2 and 3. We stop this computation at $D = 0.1$.

In the second continuation run, we change parameter C from 0 to $\frac{1}{2}$ and let D adapt. This gives us one of the two conditions for the desired far-field behaviour.

Note that in the next runs we relax the integral condition, so $N_{\mathrm{int}} = 0$ and we need just one free parameter. In the third continuation run, we change parameter A from 0 to 1, which corresponds to changing the equation from the one for determining critical nuclei to the one for determining self-similar solutions. In the fourth run, we increase the domain size to $L = 5$ while in the fifth run we change parameter D until we obtain $D = 0$. After this sequence of runs, we have obtained a solution to the self-similar film rupture problem of Section 4. In particular, both far-field boundary conditions (5.14) and (5.15) are fulfilled. The corresponding profile is given in Fig. 4. Now we can proceed and increase the domain size. Zhang & Lister (1999), for instance, employ $L = 10 \ldots 200$ while Witelski & Bernoff (1999) use $L = 25 \ldots 100$. For comparison, we produce results for the three values $L = 10$, 100 and 1000 and obtain as a result three approximations of a self-similar solution. The differences between the results obtained for these three L are very small and normally not discernible in profile plots like Fig. 4. They are better visible in quantitative measures as the value of the proportionality constant a obtained from the values on the boundary: $a = H(L)/L^{1/2}$. They are listed in the legend of Fig. 4 together with two additional values for the rather large domains $L = 10^5$ and $L = 10^6$. We note that the value for $L = 100$ agrees to 5 s.d. with the one given by Zhang & Lister (1999). The corresponding values of $H(0)$ and $H''(0)$ agree to 8 s.d. (cf. their Table II). With the exception of the fifth s.d. for a these digits remain the same when using $L = 1000$. The further increase of the domain size up to $L = 10^6$ gives a result for a that has converged for all 11 s.d. given in Fig. 4. This detailed comparison shows the viability of our numerical approach to obtain the first self-similar solution via a homotopy scheme from nucleation solutions of the related steady thin-film equation.

The self-similar solution obtained above and shown in Fig. 4 is only the first (the one of largest a) of a countably infinite sequence of such solutions. Zhang & Lister (1999) give the first six, while Witelski & Bernoff (1999) mention that they calculate the first 25. We present here a scheme that allows us to

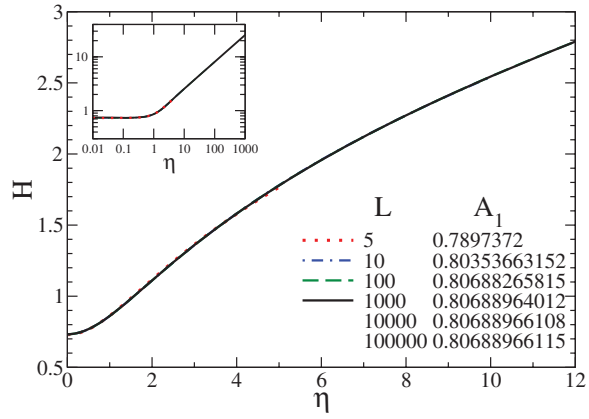

FIG. 4. The first singularity solution (largest a) is shown for several domain sizes L as indicated in the legend. The main panel gives the profiles for $\eta \in [0, 12]$ while the inset gives a log–log plot for the η up to the largest $L = 1000$. The legend also gives the values of the asymptotic proportionality factor for the first singularity solution $a = A_1$ as obtained from the value of H on the boundary: $A_1 = H(L)/L^{1/2}$.

obtain more than 40 such solutions employing readily available continuation tools in a procedure that seems to be more convenient than the ones described by Zhang & Lister (1999) and Witelski & Bernoff (1999).

We propose the following strategy to obtain a more complete sequence of self-similar solutions by a single continuation run that starts at the first self-similar solution (at some fixed L) determined above. The basic idea is to relax the condition that imposes the symmetry under parity $\eta \to -\eta$ of the self-similar solutions. In practice, we perform a continuation run where parameter B in the boundary condition for H''' at $\eta = 0$ (Equation (5.13)) is allowed to vary away from zero. This gives a continuous family of solutions with $B = y_4(0) = H'''(0)$ oscillating around zero. It is presented in Fig. 5 in various different ways. Figure 5(a) gives the complete family in the $(H(0), H''(0))$-plane, a presentation chosen by Zhang & Lister (1999). The corresponding log-log plot (Fig. 5(b)) indicates that the family of solutions first oscillates and then, at smaller $H(0)$, converges to a power law $H''(0) \sim H(0)^2$. The robustness of the procedure can be appreciated in Fig. 5(c), where we give the third derivative of H at $\eta = 0$, i.e. our continuation parameter. It is presented as a log-normal plot of the absolute value of $B = H'''(0)$ to allow us to spot zero crossings of $H'''(0)$ over many orders of magnitude. Each of the nearly vertical lines corresponds to a zero crossing and therefore to another self-similar profile. They are indicated in the other panels of Fig. 5 as triangle symbols. Inspecting Fig. 5(c) and the zoom in Fig. 6 closely, one finds that the results for $L = 100$ and $L = 1000$ virtually coincide down to about $H(0) = 0.2$. For lower values, $H'''(0)$ at the local maxima becomes smaller than 10^{-14} and cannot be resolved anymore due to numerical noise. The run shown in Fig. 5(c) gives 43 self-similar solutions. Finally, Fig. 5(d) gives the dependence of the values of the proportionality constant A_m on the solution number m in a log–log representation. In agreement with Witelski & Bernoff (1999), we find the power law dependence $A_m \sim m^{-0.46}$.

For the benefit of future comparisons between different methods, Table 1 lists for the first 15 self-similar solutions, the values obtained for $H(0)$, $H''(0)$ and the coefficient A_m. The values were obtained with $L = 1000$. The digits that agree with the results for $L = 100$ are given in bold face. The first six are

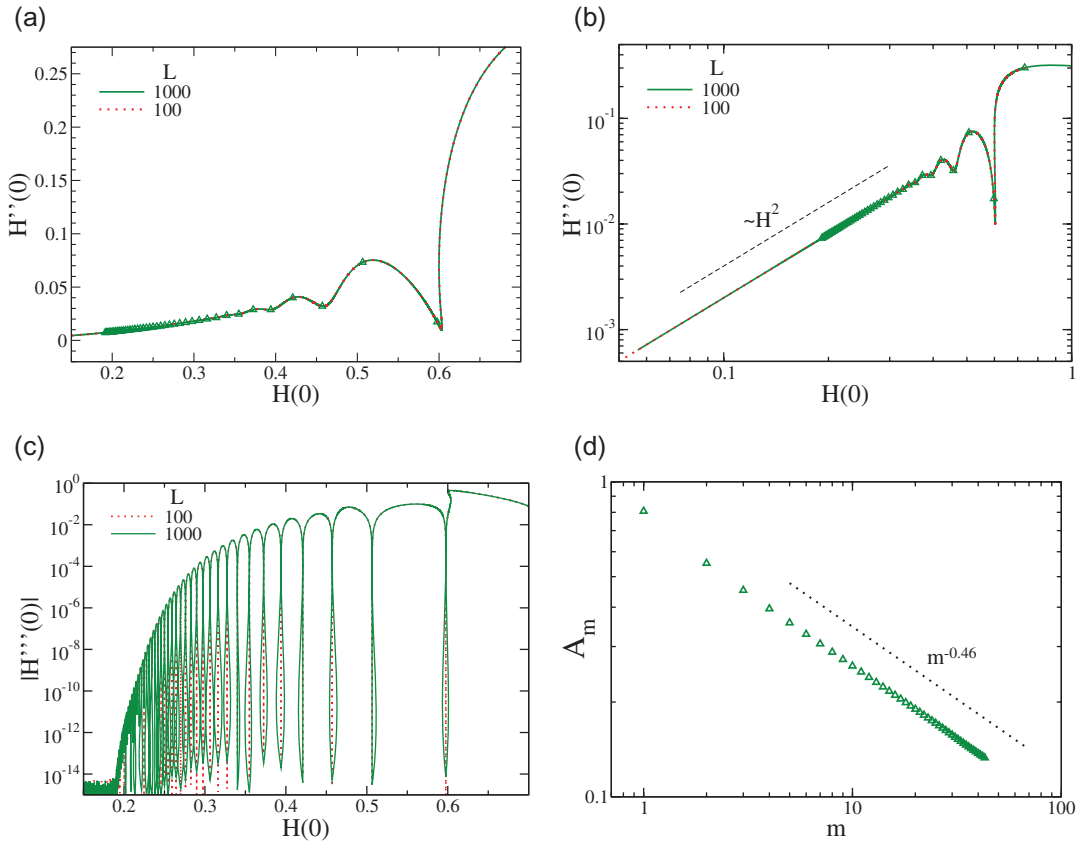

FIG. 5. Shown are various characteristics of the continuous family of solutions one obtains when relaxing the condition that the self-similar solutions are symmetric under parity. Panel (a) shows as the solid line the family in the $(H(0), H''(0))$-plane. Panel (b) gives the diamonds indicate the first 43 solutions with $H'''(0) = 0$ and hence represent self-similar reflection-symmetric solutions. (b) The same curve in a log–log plot, while (c) gives $\ln|H'''(0)|$ over $H(0)$, and (d) plots the far-field coefficient A_m over the solution number m. The first 15 self-similar profiles are given below in Fig. 7. Most results are given for $L = 100$ and $L = 1000$ as indicated in the legends.

also listed in Zhang & Lister (1999). Our discussion of Fig. 4 indicates that the results for a are exact to 7–8 s.d., while $H(0)$ and $H''(0)$ are exact to the shown 11 s.d. (which is even the case for $L = 100$).

The profiles of the first 15 self-similar solutions listed in Table 1 are shown in Fig. 7 in the form of $H(\eta)$ (panel (a)) and $H'''(\eta)$ (panel (b)). Details of the last of these solutions can only be discerned in the inset of Fig. 7(b) that zooms onto solutions 6–15. Note that the range of η that is shown is much smaller than the computational domain ($L = 100$). As noted by Zhang & Lister (1999), the profile of each successive self-similar solution shows an additional half oscillation of H''' (on the shown domain $\eta \in [0, L]$) when compared with the previous one. This implies that a 'natural' ordering of these solutions exist. Note that the first solution in Table 1 (solid black line in Fig. 7) only shows one oscillation in the interval $[0, L]$. Zhang & Lister (1999) claim that the solution with one oscillation must be the first in the sequence. Note, however, that in principle there could exist a solution with just half an oscillation, i.e. one oscillation in the interval $[-L, L]$, but such a solution was not found in our continuation run. We therefore conclude that the solution with one oscillation is indeed the first in the sequence.

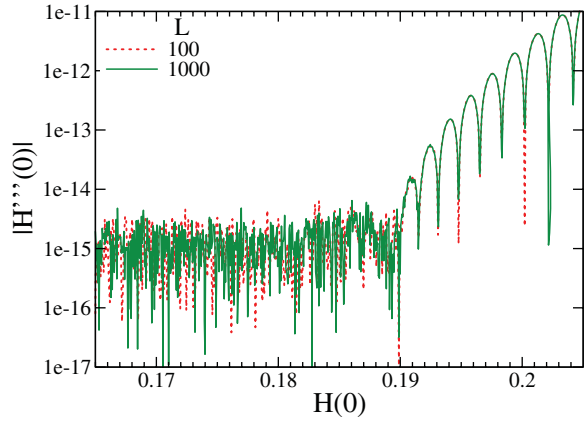

FIG. 6. A zoom into the region of Fig. 5(c) where numerical noise becomes important.

TABLE 1 *The table gives the values of* $H(0)$, $H''(0)$ *and the coefficient* A_m *for the first* 15 *self-similar solutions. The values were obtained with* $L = 1000$. *The digits that agree with the results for* $L = 100$ *are given in bold face. The values for the first six solutions were already given by Zhang & Lister (1999).*

m	$H(0)$	$H''(0)$	A_m
1	**0.73266237728**	**0.30097559166**	**0.80688**964012
2	**0.59760737292**	**0.017350716163**	**0.55135**572107
3	**0.50652965023**	**0.073219676296**	**0.45271**257812
4	**0.45718173371**	**0.032052811530**	**0.39559**087836
5	**0.42086057171**	**0.039995592383**	**0.35686**887862
6	**0.39403236690**	**0.028833236578**	**0.32827**463293
7	**0.37251867247**	**0.028847345963**	**0.30598**402843
8	**0.35494032053**	**0.024648003791**	**0.28794**339171
9	**0.34009577986**	**0.023408534458**	**0.27293**438557
10	**0.32735993193**	**0.021292784400**	**0.26018**076793
11	**0.31624154330**	**0.20072409878**	**0.24916**061052
12	**0.30642083031**	**0.18742623940**	**0.23950**786828
13	**0.29765069484**	**0.17737280897**	**0.23095**695300
14	**0.28975087198**	**0.16781841633**	**0.22330**969397
15	**0.28257992946**	**0.15974839736**	**0.21641**470686

Finally, we note that the linear stability analysis of self-similar rupture solutions performed by Witelski & Bernoff (2000) for both planar and axisymmetric problems revealed that only the first solution in the sequence is linearly stable. Therefore, only this solution is observed in time-dependent simulations of (2.1).

6. Conclusion

We have presented an alternative numerical method to obtain self-similar solutions related to the rupture of thin liquid films on a solid substrate that evolve solely under the stabilizing influence of the surface

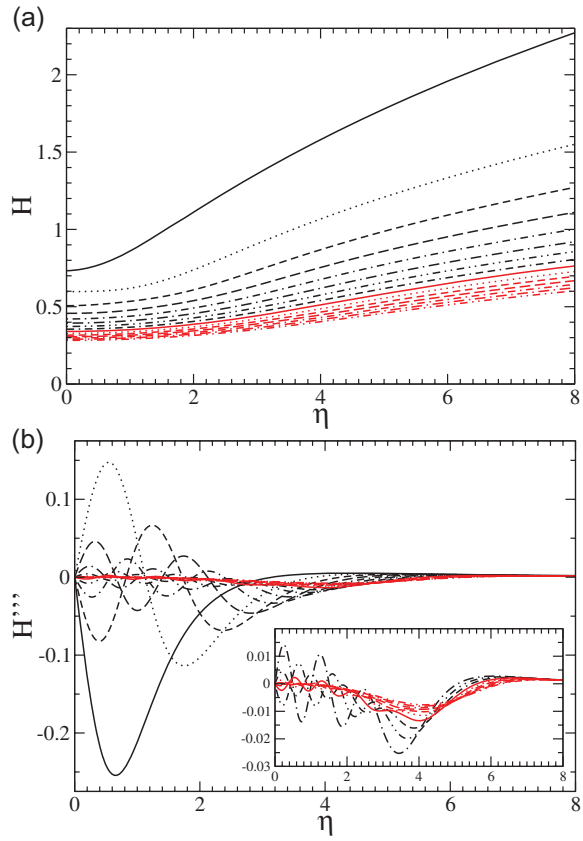

FIG. 7. The first 15 self-similar solutions are presented as (a) profiles $H(\eta)$ and (b) third derivatives $H'''(\eta)$. The inset in panel (b) zooms onto solutions 6–15 to make the fine structure better visible. Given are profiles obtained with a domain size $L = 100$ that are virtually indistinguishable from the ones obtained with $L = 1000$. Note that the shown range of η is much smaller. The sequence of line styles of (a) and (b) is identical.

tension of the free surface of the film (capillarity) and the destabilizing influence of effective van der Waals interactions between the free film surface and the substrate. This situation exactly corresponds to the one most studied in the literature, e.g. by Williams & Davis (1982), Zhang & Lister (1999) and Witelski & Bernoff (1999).

The proposed method is based on a homotopy approach that uses continuation techniques bundled in the toolbox AUTO-07P (Doedel & Oldeman, 2009) to reach the self-similar solutions related to film rupture from analytically known small-amplitude solutions of the related steady thin-film equation. In particular, we have used (i) continuation in domain size to obtain steady nucleation solutions from the analytically known starting solution; (ii) consecutive continuation in several parameters to transform the steady thin-film equation into the related equation describing self-similar rupture solutions, thereby transforming the nucleation solution into a self-similar solution and (iii) continuation in the domain size to test the validity and convergence of the obtained first self-similar solution.

The second major point has been a homotopy approach to the calculation of further members of the countably infinite set of self-similar solutions (Witelski & Bernoff, 1999). To do so, we have started

at the previously obtained first self-similar solution, have fixed the domain size and have relaxed a condition that imposes the reflection symmetry of the self-similar solutions. This has allowed us to perform a continuation in a parameter that is zero when the solution is reflection-symmetric and non-zero when it is not. Along the obtained family of solutions the parameter oscillates around zero. Each instance it crosses zero corresponds to another self-similar solution. This has, for instance, allowed us to determine more than forty self-similar solutions in a single run without much sophistication and refinement of the procedure. The approach is limited by numerical noise whose influence can surely be further suppressed (here it became dominant when the absolute value of the maxima of the oscillating continuation parameter became smaller than 10^{-14}).

The aim of the present contribution has been the presentation of a homotopy approach to the calculation of sequences of self-similar solutions. Here, we have focused on the particular case of planar (related to line rupture) self-similar solutions (related to van der Waals rupture of thin liquid films) that have a square root power law behaviour in the far-field. The approach also allows for the determination of (i) planar solutions with different far-field power law behaviour, (ii) radially symmetric self-similar solutions to the presently studied thin-film equation and (iii) self-similar solutions related to rupture for other thin-film evolution equations that show a subcritical primary bifurcation and finite-time singularities in time evolution. Potential candidates are thin films that rupture due to thermo-capillary effects (see Oron, 2000 for time integrations for rupturing films, and Thiele & Knobloch, 2004 for a study of the subcritical steady nucleation branches and related finite support droplet solutions), films of dielectric liquid in a capacitor that rupture under the influence of a DC electric field (Papageorgiou *et al.*, 2005; Verma *et al.*, 2005). Another worthwhile undertaking would be an extension of the concept towards rupture phenomena described by coupled equations as in two-layer films (Pototsky *et al.*, 2005; Ward, 2011), surfactant-covered films (Jensen & Grotberg, 1992; Matar & Kumar, 2004), free films (Vaynblat *et al.*, 2001) and films on a solid substrate in the case of a large slip (Peschka *et al.*, 2010). As a topic of future research, we also plan to investigate the usefulness of the homotopy continuation approach for analysing singularities in non-local thin-film equations (see, for example, Tseluiko & Papageorgiou, 2006, for a non-local equation arising in the study of electrified liquid films and showing infinite-time singularities).

Funding

This work was supported by the European Union under grant PITN-GA-2008-214919 (MULTIFLOW) and by the EPSRC under grant EP/J001740/1.

References

Allgower, E. L. & Georg, K. (1990) *Numerical Continuation Methods: an Introduction*. Springer Series in Computational Mathematics. Berlin: Springer.

Bonn, D., Eggers, J., Indekeu, J., Meunier, J. & Rolley, E. (2009) Wetting and spreading. *Rev. Mod. Phys.*, **81**, 739–805.

Craster, R. V. & Matar, O. K. (2009) Dynamics and stability of thin liquid films. *Rev. Mod. Phys.*, **81**, 1131–1198.

de Gennes, P.-G. (1985) Wetting: statics and dynamics. *Rev. Mod. Phys.*, **57**, 827–863.

Doedel, E., Keller, H. B. & Kernevez, J. P. (1991) Numerical analysis and control of bifurcation problems (I) Bifurcation in finite dimensions. *Int. J. Bifurcation Chaos*, **1**, 493–520.

Doedel, E. J. & Oldeman, B. E. (2009) *AUTO07p: Continuation and Bifurcation Software for Ordinary Differential Equations*. Montreal: Concordia University.

Eggers, J. (1997) Nonlinear dynamics and breakup of free-surface flows. *Rev. Mod. Phys.*, **69**, 865–929.

Erneux, T. & Davis, S. H. (1993) Nonlinear rupture of free films. *Phys. Fluids*, **5**, 1117–1122.

Grotberg, J. B. & Jensen, O. E. (2004) Biofluid mechanics in flexible tubes. *Annu. Rev. Fluid Mech.*, **36**, 121–147.
Ida, M. P. & Miksis, M. J. (1996) Thin film rupture. *Appl. Math. Lett.*, **9**, 35–40.
Israelachvili, J. N. (2011) *Intermolecular and Surface Forces*, 3rd edn. London: Academic Press.
Jensen, O. E. & Grotberg, J. B. (1992) Insoluble surfactant spreading on a thin viscous film: shock evolution and film rupture. *J. Fluid Mech.*, **240**, 259–288.
Laugesen, R. & Pugh, M. (2000) Linear stability of steady states for thin film and Cahn–Hilliard type equations. *Arch. Ration. Mech. Anal.*, **154**, 3–51.
Laugesen, R. S. & Pugh, M. C. (2002) Energy levels of steady states for thin-film-type equations. *J. Differential Equations*, **182**, 377–415.
Matar, O. & Kumar, S. (2004) Rupture of a surfactant-covered thin liquid film on a flexible wall. *SIAM J. Appl. Math.*, **64**, 2144–2166.
Oron, A. (2000) Nonlinear dynamics of three-dimensional long-wave Marangoni instability in thin liquid films. *Phys. Fluids*, **12**, 1633–1645.
Oron, A., Davis, S. H. & Bankoff, S. G. (1997) Long-scale evolution of thin liquid films. *Rev. Mod. Phys.*, **69**, 931–980.
Papageorgiou, D. T. (1995) On the breakup of viscous liquid threads. *Phys. Fluids*, **7**, 1529–1544.
Papageorgiou, D. T., Petropoulos, P. G. & Vanden-Broeck, J. M. (2005) Gravity capillary waves in fluid layers under normal electric fields. *Phys. Rev. E*, **72**, 051601.
Peschka, D., Münch, A. & Niethammer, B. (2010) Thin-film rupture for large slip. *J. Engrg. Math.*, **66**, 33–51.
Pototsky, A., Bestehorn, M., Merkt, D. & Thiele, U. (2005) Morphology changes in the evolution of liquid two-layer films. *J. Chem. Phys.*, **122**, 224711.
Sharma, A. & Ruckenstein, E. (1985) Mechanism of tear film rupture and its implications for contact-lens tolerance. *Amer. J. Optom. Physiol. Opt.*, **62**, 246–253.
Starov, V. M. & Velarde, M. G. (2009) Surface forces and wetting phenomena. *J. Phys.-Condens. Matter*, **21**, 464121.
Thiele, U. (2010) Thin film evolution equations from (evaporating) dewetting liquid layers to epitaxial growth. *J. Phys.-Condens. Matter*, **22**, 084019.
Thiele, U. & Knobloch, E. (2004) Thin liquid films on a slightly inclined heated plate. *Phys. D*, **190**, 213–248.
Tseluiko, D. & Papageorgiou, D. T. (2006) Nonlinear dynamics of electrified thin liquid films. *SIAM J. Appl. Math.*, **67**, 1310–1329.
Vaynblat, D., Lister, J. R. & Witelski, T. P. (2001) Rupture of thin viscous films by van der Waals forces: evolution and self-similarity. *Phys. Fluids*, **13**, 1130–1140.
Verma, R., Sharma, A., Kargupta, K. & Bhaumik, J. (2005) Electric field induced instability and pattern formation in thin liquid films. *Langmuir*, **21**, 3710–3721.
Ward, M. H. (2011) Interfacial thin films rupture and self-similarity. *Phys. Fluids*, **23**, 062105.
Williams, M. B. & Davis, S. H. (1982) Nonlinear theory of film rupture. *J. Colloid Interface Sci.*, **90**, 220–228.
Witelski, T. & Bernoff, A. (1999) Stability of self-similar solutions for van der Waals driven thin film rupture. *Phys. Fluids*, **11**, 2443–2445.
Witelski, T. & Bernoff, A. (2000) Dynamics of three-dimensional thin film rupture. *Physica D*, **147**, 155–176.
Zhang, W. & Lister, J. (1999) Similarity solutions for van der Waals rupture of a thin film on a solid substrate. *Phys. Fluids*, **11**, 2454–2462.